Proceedings of ASME Turbo Expo 2011
GT2011
June 6-10, 2011, Vancouver, British Columbia, Canada

GT2011-46217

DETAILED COLD-FLOW SIMULATION TO ESTIMATE MASS FLOW DISTRIBUTION OF AIRCRAFT COMBUSTOR

Mitsumasa Makida
Aviation Program Group,
Japan Aerospace Exploration Agency
7-44-1 Jindaiji-higashi, Chofu, Tokyo, JAPAN 182-8522

Naoki Nakamura
Advanced Science & Intelligence Research Institute
1-18-14 Uchi-Kanda, Chiyoda, Tokyo, JAPAN 101-0047

Osamu Nozaki
Aircraft Propulsion Research Center,
Japan Aerospace Exploration Agency
7-44-1 Jindaiji-higashi, Chofu, Tokyo, JAPAN 182-8522

ABSTRACT

In the TechCLEAN project of JAXA, a combustor for a small aircraft engine has been developed. The combustor was tuned to show the behavior of the Rich-Lean combustion through combustion tests under atmospheric and practical conditions. Finally, the full annular combustor was successfully tuned to reduce NOx emissions to 38.1% of the ICAO CAEP4 standard under ICAO LTO cycles, also sustaining basic performances as an aircraft combustor.

In the development process of the combustor, numerical simulation methods were also utilized as analysis tools to accelerate the development of the combustor. To use them in the screening process of the combustor design, we focused on cost-effective simulation methods adopting the cold-flow RANS simulation code UPACS which has been developed in JAXA. Moreover, to simplify the treatment of calculation grids of the combustor with complicated configuration, we also utilized combination of the overset grid method and the attached multi-block grid method.

In the previous report, we introduced the overview of the application of the cold-flow simulation in the combustor development process. Subsequently, in this report, we focus on the effect of combustor configuration parameters to the air mass flow ratio among fuel nozzles, dilution air holes and cooling air holes on the combustor linear. Then we also show the estimation method of the effective open area of combustor liners, mass flow ratio between air holes, and total pressure loss of the combustor.

NOMENCLATURE

Ai	Actual area of air hole i
CAEP	Committee on Aviation Environmental Protection
Cdi	Overall discharge coefficient of air hole i
FA	Full annular
ICAO	International civil aviation organization
LTO	Landing and take-off
MSU	Multi-sector unit
ΔP	Pressure difference
SSU	Single-sector unit
Wa	Inlet mass flow rate of 1/16 single-sector
ρ	Air density

1 INTRODUCTION

In general, small and medium power aircraft engines must simultaneously satisfy several requirements, for example, high efficiency, environmental friendliness and cost effectiveness [1]. In October 2003, Japan Aerospace Exploration Agency (JAXA) started a project "Technology development project for clean engines" (so-called TechCLEAN project), in which researches to develop advanced combustion technology were conducted aiming to reduce toxic exhaust gas components, especially NOx, from aeroengine combustors. In the framework of the TechCLEAN project, JAXA has been developing aeroengine combustors for an affordable and environment-friendly small aircraft (with approximately 50-passengers). The designed thrust of the engine is about 40kN and the pressure

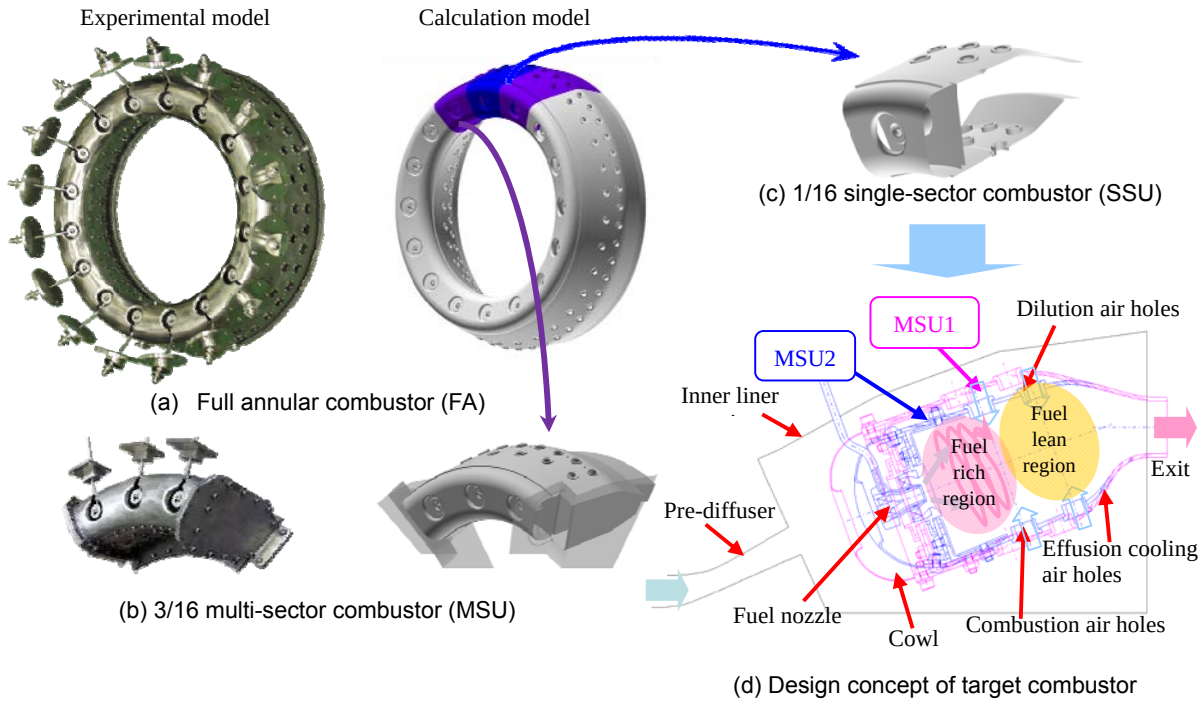

Fig.1 Target aircraft combustor models and calculated region with schematic sectional drawing.

ratio is about 20. The target of the combustor development is to reduce NOx emissions lower than 50% of the ICAO CAEP4 standard, aiming to precede the trend of NOx emissions, also to reduce CO and UHC emissions to those of 90% and to ensure basic performance of aero engine combustors, such as ignition and blow-out.

We started from preliminary combustion tests with tubular combustors under atmospheric conditions. Both model combustors and test conditions got closer to the target engine combustor step by step, and finally full annular combustors were tested under practical conditions and succeeded to reduce NOx emissions to 38.1% of the ICAO CAEP4 standard [2-4]. Although the development of our combustor was mainly conducted through experimental research, we also tried to utilize numerical simulation methods as design tools to accelerate the combustor development process. As combustion experiments require plenty of costs and time, it is difficult to conduct parametric experiments for many combustor models. So, we made efforts to find the way to utilize cost-effective numerical simulations, which can be used for the screening process in the preliminary design phase.

In general, an aircraft combustor consists of many components such as cowls, fuel nozzles, swirl vanes and dilution air holes, therefore its configuration is very complicated. In addition, the evaporation and combustion phenomena of the liquid fuel in the combustion chamber should be treated simultaneously. Much research has been conducted to simulate the phenomena inside the combustor; from early research for basic combustor models [5,6] to recent practical applications [7-15]. Unfortunately, it is still difficult to get exact solution over the whole combustor region within limited time and cost. Because our objective of applying numerical simulations in the development process was to find the cost-effective method which can be utilized to reduce the cost of experiments, we adopted the cold-flow simulation method. Even if the target solution is limited to the flow-field, it should change as the temperature gets higher with combustion, so the cold-flow simulation cannot give the exact solution in the combustor. By taking these effects into consideration, we could get some information that is required in the preliminary design process of the combustor, through the cold-flow simulation.

2 TARGET COMBUSTOR MODELS

Experimental and calculation models of our combustors are shown in Fig.1; (a) full annular combustors and (b) multi-sector combustors. Full annular combustors of our design consist of 16 sector regions, which include one fuel nozzle respectively. In general, full annular combustors would not be tested in the early stage of combustor development process. Before that, some models of single sector combustors with one fuel nozzle and multi-sector combustors with two or three fuel nozzles would be tested, and they are tuned to show appropriate performance as aero engine combustors. Then full annular combustors are designed based on previous combustor models and tested. Also in the numerical simulation, cost effective parametric studies of single-sector combustors, as shown in Fig.1c, are mainly conducted. Then the calculation models

Table 1 List of calculation and experimental combustor models with configuration parameters.
(Cells of parameters modified from previous model are filled with blue.)

Calculation model	Liner	Cowl	Air hole size and number (st.: staggered)				Experimental model	
			Combustion	Dilution		Cooling	MSU	FA
Single-sector Calculation Model								
S1h1	L1	C1	φ10.2x4	φ9.4x6			MSU1	
S1h2	L1	C1	φ10.2x4	φ11.4x6				
S1h2c2	L1	C2	φ10.2x4	φ11.4x6				
S1h2c3	L1	C3	φ10.2x4	φ11.4x6				
S2h2	L2	C1	φ10.2x4	φ11.4x6				
S2h2st	L2	C1	φ10.2x4 st.	φ11.4x6				
S2h3st	L2	C1	φ10.8x4 st.	φ11.4x6	φ3.5x4		MSU2	FA1-1
S2h3stcool	L2	C1	φ10.8x4 st.	φ11.4x6	φ3.5x4	φ3.3x46	MSU2	FA1-1
S2h4st	L2	C1	φ10.2x4 st.(Trans.)	φ10.9x6	φ3.5x4			FA1-2
Multi-sector Calculation Model								
M2h3st	L2(x3)	C1	φ10.8x4 st.	φ11.4x6	φ3.5x4		MSU2	

would be extended to (b) multi-sector combustors, and also would be extended to (a) full annular combustors.

On the other hand, as shown in Fig.1d, the combustor consists of many components such as cowl, fuel nozzle with swirl vanes, and air holes on the combustor liner. Because the Rich-Lean combustion concept [16] was applied to our combustor to reduce NOx emissions, only about 10% of the total air goes through the fuel nozzle, that is, most of the air goes through air holes on the combustor liner. Therefore, the estimation and tuning of air flow ratio going through the combustion and dilution air holes becomes very important. A lot of research has been done on these factors [17-24], and also in our experimental research, a large portion of effort has been concentrated on them. So in this study, we selected the size, number and allocation of these air holes as configuration parameters of the screening process by numerical simulation. Additionally, the calculation range covers whole combustor region including pre-diffuser, cowl, fuel nozzle, combustion and dilution air holes and combustor liners. Although, the effusion cooling air holes on the combustor liners were omitted in calculation models to suppress the calculation costs, with the exception of one calculation model.

For experimental combustor models to be simulated, we selected multi-sector combustors MSU1 and MSU2, and full annular combustors FA1-1 and FA1-2. Here, MSU2 was modified from MSU1 aiming to reduce total pressure loss of the combustor to that of the design point, by changing the liner shape as shown in Fig.1d, and also enlarging the size of combustion and dilution air holes. Then FA1-1 was designed based on the single-sector region of MSU2, with the same size and number of air holes. Through successive experimental and numerical tests, FA1-1 was modified to the second full annular combustor model FA1-2, by tuning the size of air holes.

Calculation combustor models are listed in Table 1. Some models (filled with green) are corresponded to experimental models mentioned above. The meaning of filled color for experimental models (red, yellow and purple) will be mentioned later in section 4.4. As shown in this table, configuration parameters such as the shape of combustor liner and cowl, the size and allocation of combustion and dilution air holes, and the existence of cooling air holes are varied among those calculation models. Cells of parameters modified from the previous model are filled with blue.

3 CALCULATION METHOD

In order to apply to the screening process in the preliminary design phase, we chose the cost-effective simulation method which can be applied to many combustor models within limited time and cost. Although this method was already introduced in the previous report [25], some information that is required to understand the feature of the calculation is explained here again. For the simulation code, we adopted UPACS (Unified Platform for Aerospace Computational Simulation) code, which has been developed in JAXA [26]. UPACS solves three-dimensional compressible RANS equations under perfect gas assumptions, based on the cell-centered finite volume method. For discretization methods, implicit Roe's approximate Riemann solver with 2nd-order MUSCL (Monotone Upstream-centered Schemes for Conservation Laws) interpolation is applied for the convection terms, and 2nd-order central difference is applied for those of diffusion terms. Then they are integrated in time by matrix free

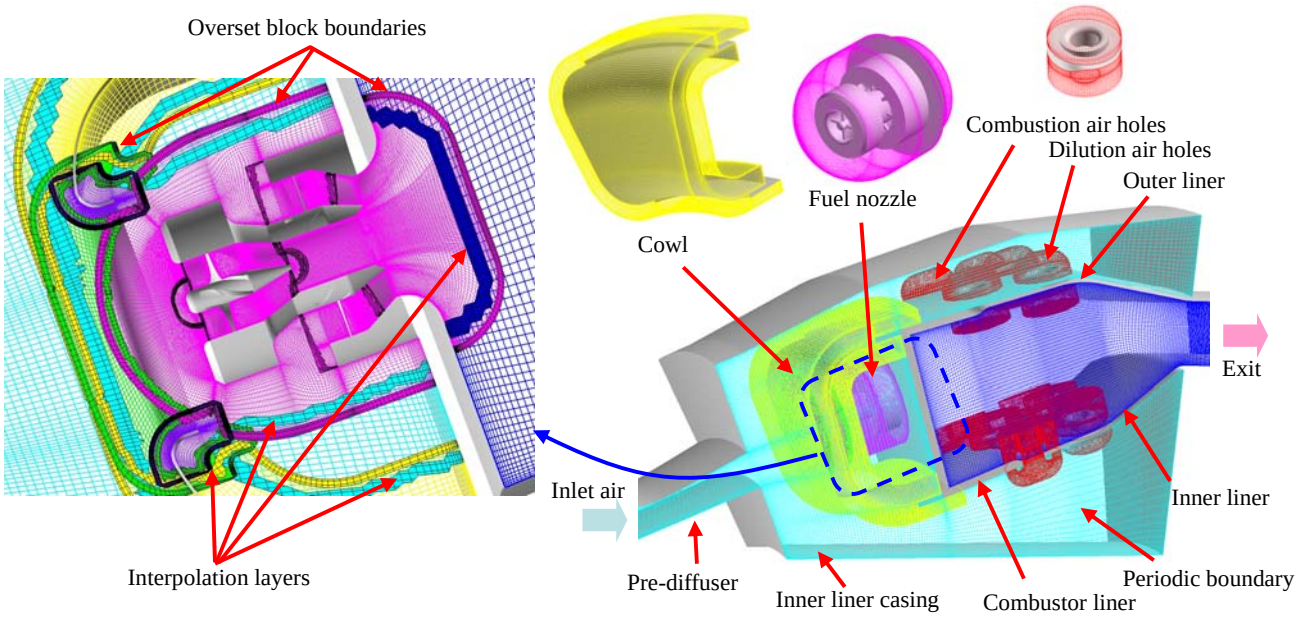

Fig.2 Setup of combustor calculation grids and generated interpolation layer along overset boundary.

Gauss-Seidel scheme with variable local time steps. The calculation was conducted until the solution converges to the steady state. As for the turbulence model, we applied the Spalart-Allmaras model [27].

In addition, as mentioned before, the combustor consists of many components as shown in Fig.1d. Therefore, in the screening process of the combustor design, in order to easily change not only the configuration of liner and cowl but also the size and allocation of air holes, we applied the overset grid method embedded in UPACS code [28]. This method enables us to handle these combustor components as separate parts. Using the combination of overset grid method with attached multi-block grid method, calculation grids of our combustor was generated as shown in Fig.2. The calculation region includes combustor liners, extracting the 1/16 single-sector region from the full annular combustor as shown in Fig.1c, attached with a fuel nozzle, a pre-diffuser and a liner casing. Grids for the regions inside and outside the combustor liner are set as background grid groups, and front grid groups are generated around the cowl, the fuel nozzle and air holes. Overset block boundaries are set around the front grid groups, and then the interpolation layers in the background grid groups are generated automatically along the overset boundaries. Then data can be transferred among overlapped grid groups. Detail of the overset situation around the fuel nozzle is shown in the left of Fig.2, and we can see interpolation layers with the thickness of two cells are generated along the inner side of the overset block boundaries. As the overlapped region should include both the overset grid boundary and the interpolation layer, the thickness of the overlapped region should be more than 10 cells. The detail of the generation of overlapped grids is described in the reference [28]. As the large part of the pressure loss inside the combustor is assumed to be generated near casing and liner walls, the calculation grid was carefully generated, concentrating near wall boundaries, and the value of $y+$ was suppressed to about 3. This made the total number of grid points of the calculation grids increase to about 12 million for the single-sector combustor region. For other boundary conditions, the circumferentially divided boundaries are set to periodic boundaries. Besides, the inlet air condition is adjusted to the experiments as will be mentioned in section 4.1. For example, under the condition of pressure difference with 9%, the Reynolds number is about 47000 and the swirl number is

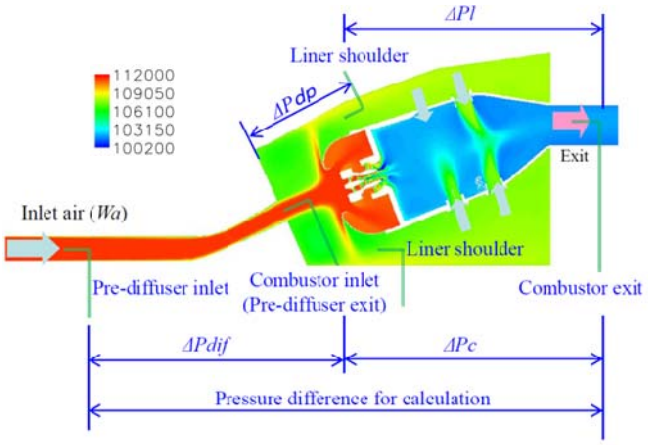

Fig.3 Definition of pressure measurement points and pressure differences.
(Shown with total pressure distribution (Pa).)

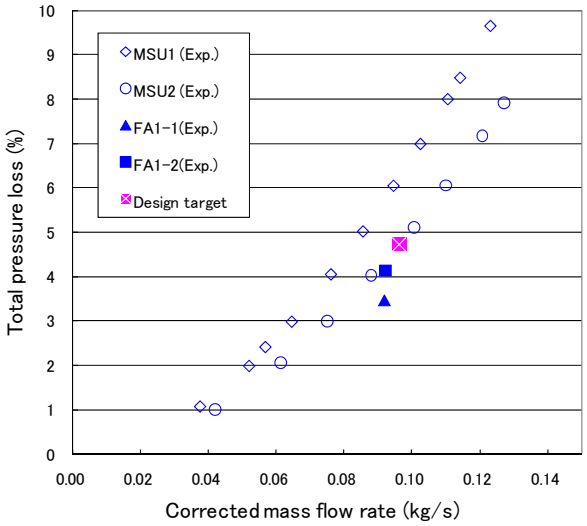

Fig.4 Relation between air mass flow rate and total pressure loss for experimental models.

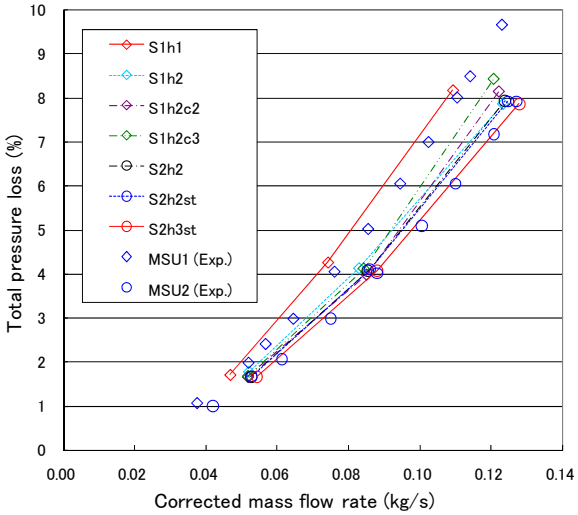

Fig.5 Effect of combustor configuration on total pressure loss of calculation models.
(Shown with experimental models MSU1 and MSU2.)

about 0.5 near the exit of the fuel nozzle.

On the other hand, for the purpose of flow-field simulation inside aeroengine combustors with complicated configurations, unstructured grid methods also can be adopted. However, in that case, only to change the size of one air hole, we might regenerate grids over the wide region. So, even there should be some interpolation errors across the overset boundaries, we chose simpler and more convenient method; the combination of the overset grid method with the attached multi-block grid method.

4 RESULTS AND DISCUSSION

4.1 Relation Between Air Mass Flow and Total Pressure Loss

For calculation and experimental combustor models listed in Table 1, inlet mass flow rate and total pressure loss of the combustor were obtained. The definition of pressure differences are shown in Fig.3 with an example of total pressure distribution on the center plane. For experimental models, the pressure difference between the pre-diffuser exit and the combustor exit ΔPc, and the mass flow of inlet air Wa were measured. Those of multi-sector combustors MSU1 and MSU2 were measured under atmospheric pressure condition with inlet temperature of 500K, varying the pressure difference ΔPc between 1% and 9%. In contrast, those for full annular combustors FA1-1 and FA1-2 were measured at only one condition of the design point of the target engine. On the other hand, for calculation models, the inlet air condition was also adjusted to atmospheric test; temperature was set to 500K and the pressure difference between the pre-diffuser inlet and the combustor exit was set between 1% and 9%. For both experimental and calculation models, the total pressure loss of the combustor was defined between the pre-diffuser exit and the combustor exit, that is, ΔPc. Then obtained inlet mass flow rate Wa was corrected by the equation below;

$$Wa_{cr} = Wa\sqrt{\frac{T}{T_{ref}}}\Big/\frac{P}{P_{ref}} \qquad (1)$$

Here, subscript "*ref*" means the reference state, where T_{ref}=288.15K and P_{ref}= 0.1013MPa. The relation between obtained air mass flow rate and total pressure loss of experimental models is plotted in Fig.4, with the design target of total pressure loss under non-combustion condition.

4.2 Effect of Configuration Parameters

In the development process of 3/16 multi-sector combustors, the first experimental model MSU1 was designed and tested, but as shown in Fig.4, its total pressure loss was higher than the target value. So to reduce the pressure loss in the second model MSU2, the combustion and dilution air holes were enlarged and the liner height of the combustor was lowered as shown in Fig.1d. Then in the experiment of MSU2, the total pressure loss was successfully got closer to the design value as shown in Fig.4. Meanwhile, because both the air hole size and the liner height were modified at once, we could not specify which modification mainly contributed to the reduction of the total pressure loss. Therefore, we conducted cold-flow simulations changing these configuration parameters individually. The detail of this discussion was already reported in the previous report [25], but the results will be mentioned here again briefly, showing the variation of relationship between corrected air mass flow rate and total pressure loss in Fig.5.

As shown in Table 1, calculation models S1h1 and S2h3st correspond to experimental models MSU1 and MSU2 respectively. Then configuration parameters were varied between them individually for calculation models from S1h2 to

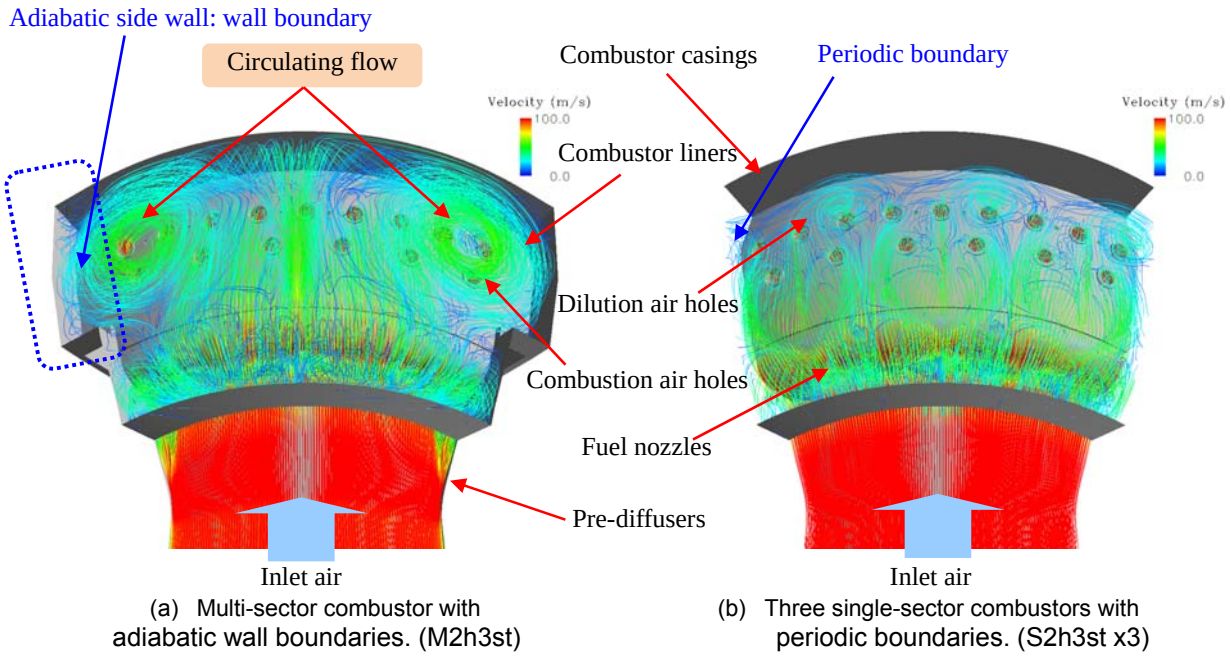

Fig.6 Comparison between multi-sector and ideal full annular combustor models.

S2h2st. The size of dilution air holes was enlarged for S1h2, and the shape of the cowl was sharpened from S1h2 to S1h2c2 and S1h2c3. Then the liner height was lowered from S1h2 to S2h2, to the height of MSU2. We can see from Fig.5 that the pressure loss of S1h2, S1h2c2, S1h2c3 and S2h2 were close. In other words, the enlargement of dilution air holes mainly contributed to the reduction of the total pressure loss. In addition, the allocation of combustion air holes was changed to staggered type for S2h2st, and also the combustion air holes are enlarged and small dilution air holes were added between original dilution air holes for S2h3st. As shown in Fig.5, the pressure loss was reduced further from that of S2h2st by this modification. Besides, in Fig.5, total pressure loss of experimental models MSU1 and MSU2 are plotted again for reference. Plots of corresponding experimental models MSU1, MSU2 and S1h1, S2h3st were close respectively, but as mentioned before, effusion cooling air holes on combustor liners, of which total open area is equivalent to about 20% of that of the whole combustor, were omitted in calculation models, pressure loss of S1h1 and S2h3st should be much higher than MSU1 and MSU2. The reason of this underestimation will be shown in the following section 4.3.

4.3 Difference Between Multi-sector and Full Annular Combustors

Following experimental and numerical results of multi-sector combustors, the first experimental model of full annular combustor FA1-1 was designed based on the multi-sector model MSU2. As already shown in Fig.4, the total pressure loss of FA1-1 was rather lower than expected from the experimental results of MSU2, which was close to the design target. Additionally, some differences were also observed in the combustion characteristics, especially for NOx emissions [25]. To investigate the difference between FA1-1 and MSU2, we focused on the experimental configurations of MSU2. The multi-sector combustor MSU2 was attached with adiabatic walls at both sides, as shown in Fig.1b. Therefore we also made the calculation model M2h3st, combining three calculation grids of 1/16 single-sector models S2h3st, and added additional region outside of two side walls instead of periodic boundaries as shown in Fig.6a. Then compared it with the ideal full annular configuration consists of three 1/16 single-sector models S2h3st with periodic boundaries, as shown in Fig.6b. Calculated streamlines colored by gas velocity magnitude are shown in Fig.6 for both calculation models. In Fig.6a, we can see that two large circulating flows exist near the attached wall regions. So we guessed that this caused additional pressure loss in the region between casings and liners, therefore reduced air flow ratio passing through the combustion and dilution air holes. In other words, the calculated mass flow ratio through fuel nozzles of M2h3st was guessed to be larger than that of S2h3st. Aiming to modify the mass flow ratio of S2h3st closer to that of M2h3st, we made another calculation model S2h4st, reducing the size of both combustion and dilution air holes as shown in the lower line of Table 1. Moreover, the arrangement of combustion air holes was transposed between inner and outer liners, in accordance with the experimental model FA1-2.

In Fig.7, circumferential distribution of mass flow ratio through the combustion and dilution air holes on both outer and inner liners, which are defined in Fig.2, are compared among M2h3st, S2h3st and S2h4st models. Here, the vertical axis shows the ratio of each air mass flow divided by the total air

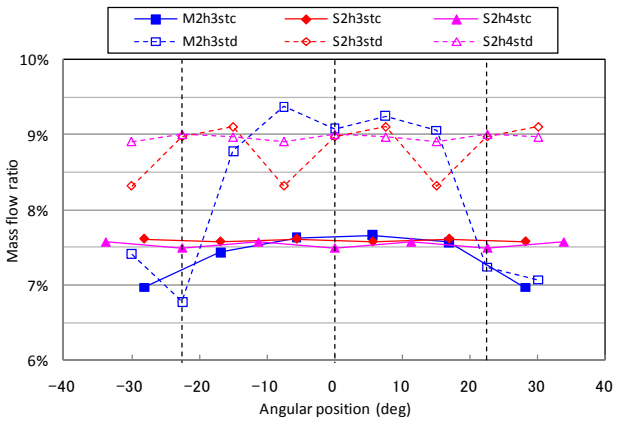

(a) Distribution on outer liner

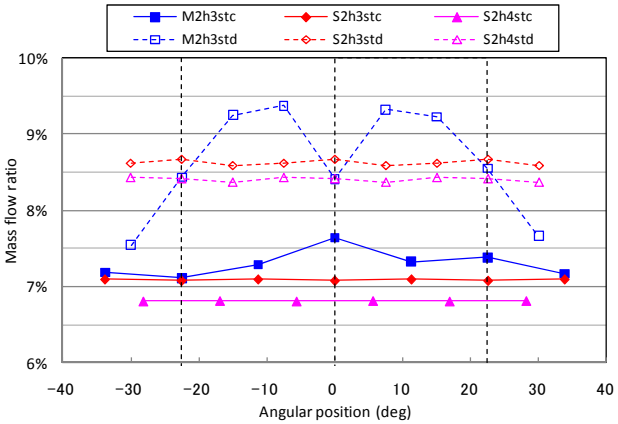

(b) Distribution on inner liner

Fig.7 Comparison of mass flow ratio distribution among multi-sector and ideal full annular combustor models. (-c: combustion air holes, -d: dilution air holes.)

mass flow from the pre-diffuser inlet. The lateral axis shows the circumferential angular position, setting the angle of the center fuel nozzles to 0 degree. Here, three vertical dotted lines indicate the center of three fuel nozzles respectively. For S2h3st and S2h4st models, three same results are plotted repeatedly. From these plots, we can see that the mass flow through the dilution air holes of the M2h3st model was reduced near both adiabatic boundaries, which means, the air flow to the downstream was disturbed by the circulating flows near the attached wall regions. In addition, comparisons of air mass flow ratio through total fuel nozzles, combustion and dilution air holes among three calculation models are also shown in Fig.8. The mass flow ratio through the fuel nozzle of S2h3st model was reduced tenth from that of M2h3st, and this is also guessed to be one of the reasons of pressure loss reduction. The mass flow ratio through the fuel nozzle was recovered by half for the S2h4st model, and as shown in Fig.9, the total pressure loss was also recovered between M2h3st and S2h3st. Based on this result, we designed the second experimental full annular

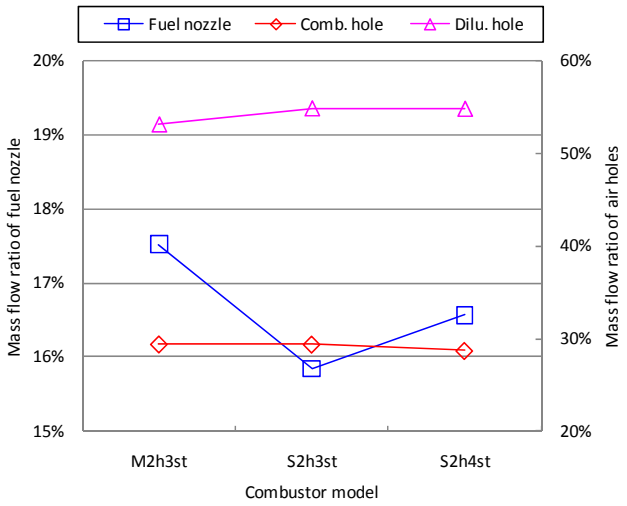

Fig.8 Comparison of mass flow ratio among multi-sector and ideal full annular combustor models.

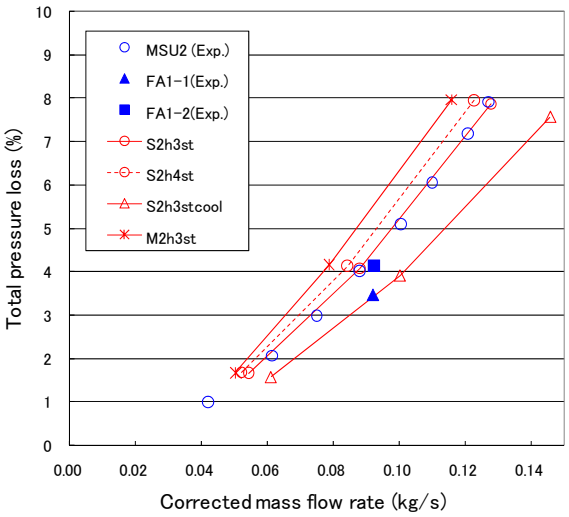

Fig.9 Comparison of total pressure loss among multi-sector and ideal full annular combustor models. (Shown with experimental models and calculation model S2h3stcool.)

combustor model FA1-2, reducing the size of the combustion and dilution air holes to that of S2h4st. In the combustion tests of FA1-2 under practical conditions, the total pressure loss increased near the design target as shown in Fig.9, and also the combustion characteristics successfully got closer to that of MSU2 [25].

In addition, from these experimental and calculation results, we can say that, in the experiment of multi-sector combustors, the side wall regions should be treated carefully. Otherwise the pressure loss and air flow distribution would largely differ from those of full annular combustors, which

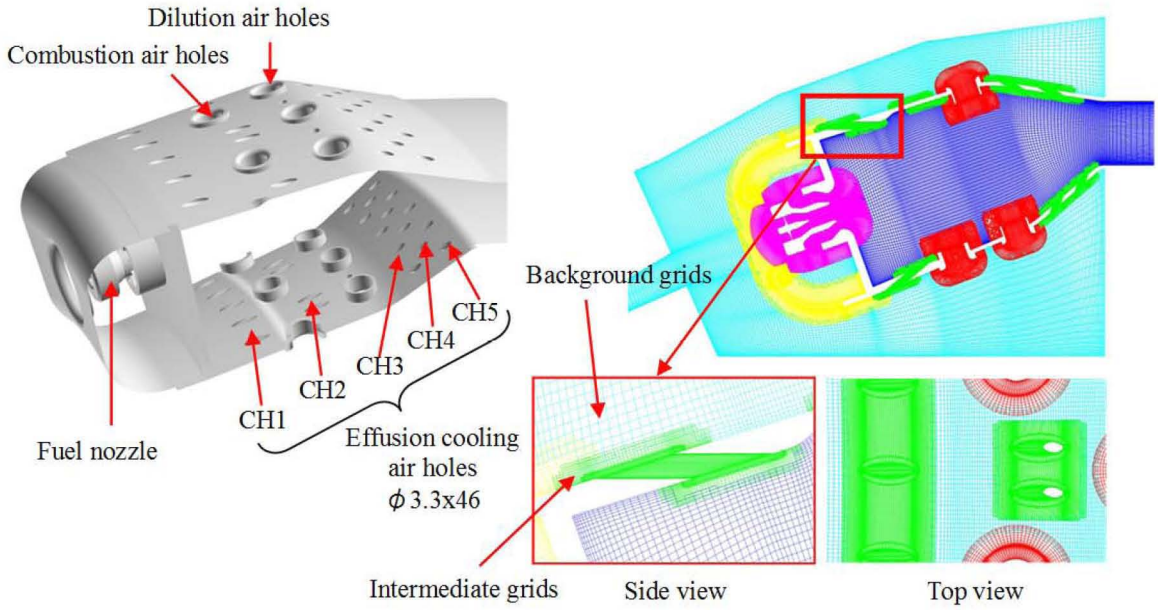

Fig.10 Setup of combustor calculation grids of S2h3stcool including effusion cooling air holes.

would cause the difference in the combustion characteristics. We also got some guidelines to correct the difference.

Meanwhile, pressure loss of experimental models MSU2, FA1-1 and FA1-2 are plotted again in Fig.9 for comparison. The difference between corresponding models; MSU2 and M2h3st, FA1-1 and S2h3st, FA1-2 and S2h4st got closer, but likewise Fig.5, there were still differences caused by the omission of cooling air holes in calculation models. In the following section, this difference tried to be reduced by the calculation model S2h3stcool, as also plotted in Fig.9.

4.4 Effect of Effusion Cooling Air Holes

As mentioned before, because of calculation costs, effusion cooling air holes on combustor liners were omitted for all calculation models reported previously. Besides, to estimate the air mass flow ratio among the fuel nozzle and air holes on the combustor liner, by adjusting the effective open area on the combustor liner, cooling air holes were included in the calculation model S2h3stcool, and the effect of these holes was investigated.

The configuration and the overset grid construction of S2h3stcool model are shown in Fig.10. For the corresponding experimental model FA1-1, more than 200 cooling air holes of 1mm diameter were drilled on the combustor liner within the single-sector region. As for S2h3stcool, 46 air holes of 3.3mm diameter were put on the combustor liners, adjusting the total area of cooling air holes, that is, adjusting mass flux ratio to that of FA1-1. Although, to investigate the effect of cooling air hole position, air holes were separated into five groups, as shown in the left of Fig.10, named from upstream as CH1 to CH5. Calculation grids of these cooling air holes were connected to background grids inside and outside the combustor liner, through intermediate grids as shown in the right of Fig.10. By adding cooling air holes, the total number of grid points was increased to about 26 million. The resulting total pressure loss is plotted in Fig.9, and it is almost coincident with the plot of the experimental model FA1-1.

In addition, to investigate the distribution of air mass flow ratio through cooling air holes, the circumferential distribution of overall discharge coefficient for all cooling air hole groups CH1 to CH5 are plotted in Fig.11, also distinguished between inner(-i) and outer(-o) liner groups. Here, the detailed definition

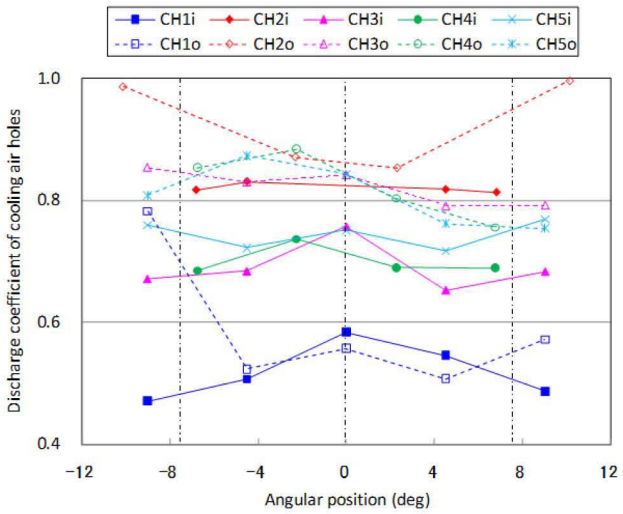

Fig.11 Distribution of overall discharge coefficient of effusion cooling air holes. (-i: inner liner, -o: outer liner.)

Table 2 Overall Discharge coefficient of fuel nozzles and air holes for calculation models.

		S2h2st	S2h3st	S2h4st	S2h3stcool	M2h3st
Fuel nozzle		1.72	1.73	1.73	1.76	1.73
Combustion air holes		0.84	0.83	0.84	0.81	0.72
Dilution air holes		0.90	0.89	0.90	0.88	0.74
Small dilution air holes		-	0.68	0.66	0.68	0.59
Effusion cooling air holes						
CH1		-	-	-	0.55	-
CH2	Inner	-	-	-	0.82	-
	Outer	-	-	-	0.93	-
CH3, 4, 5	Inner	-	-	-	0.71	-
	Outer	-	-	-	0.82	-

of "overall" will be described in the following section 4.5. We can see from these plots, that even the circumferential fluctuation was not large except for one case (CH1o), there were large differences among cooling air hole groups. Also in comparison with inner and outer cooling air holes, similar to combustion and dilution air holes shown in Fig.7, outer mass flow was larger than that of inner. These differences should be taken into account in the estimation of effective open area of the combustor liners, in the design process of the combustor.

Here, the difference of cell color for experimental models in Table 1 can be explained. First, for red cells, the corresponding calculation models simulate only combustion and dilution air holes. Secondly, for yellow cells, combustor configuration, with or without adiabatic wall boundaries, are additionally simulated. Thirdly, for the purple cell (S2h3stcool only), effective open area on combustor liners are also adjusted in the calculation model, by including cooling air holes. As shown in Fig.9, calculation with cooling air holes simulates the experimental models well, but this simulation takes much resources. So, in the next section, we demonstrate the way to estimate the total pressure loss, mass flow balance and distribution of mass flow ratio, utilizing the detailed information obtained from the heavy calculation of S2h3stcool.

4.5 Estimation of Effective Opening Area and Total Pressure Loss of Combustion Liner

In general, in the design process of air craft combustors, as shown in previous sections, the estimation of effective open area is very important. It directly affects the relation between the inlet air mass flow rate and the total pressure loss, and also affects the mass flow ratio among fuel nozzles and air holes on the combustor liner. So, we tried to obtain information from cold-flow calculations to support the estimation.

From the results of calculation, we sampled the total pressure at shoulders of the combustor liner as shown in Fig.3, and estimated the pressure difference through the liner ΔP_l. For each air hole i on the combustion liner, including combustion, dilution and effusion cooling air holes, the air mass flow rate Wa_i through it was sampled respectively. Then overall discharge coefficient for each air hole Cd_i was estimated by the equation for incompressible flow calculations;

$$Cd_i = Wa_i \Big/ \sqrt{2\rho\Delta P_l} \Big/ A_i \qquad (2)$$

Here "overall" means that the pressure difference ΔP_l includes the pressure loss caused by the linear casing and the mixing flow inside the combustor, and A_i means actual area of each air hole. Similarly, Cd_i of the fuel nozzle with swirl vanes was also estimated by replacing ΔP_l with ΔPc in equation (2), and the effective open area, experimentally measured separately, was substituted for A_i. Resulting Cd_i are listed for some calculation models in Table 2. We can see that Cd_i of fuel nozzles exceeds 1. This is because, as shown in Fig.3, high total pressure at the inlet of fuel nozzle leads to increase the mass flow through swirl vanes. We can also see that the change of size and number of air holes, even the addition of effusion air holes, do not largely affect the estimated discharge coefficients of fuel nozzles, combustion and dilution air holes. However, for the

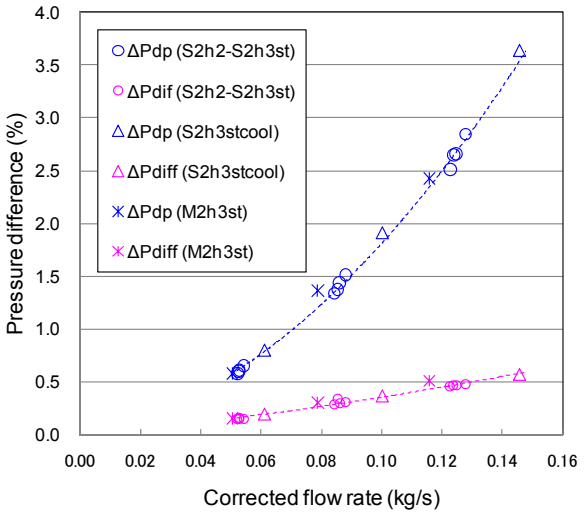

Fig.12 Relation between mass flow rate and pressure difference through pre-diffuser and dump region.

multi-sector model M2h3st, coefficients of combustion and dilution air holes are decreased, in accordance with the decrease of mass flow through the liner, which was described in section 4.3. Also as already shown in Fig.11, Cd_i of effusion cooling air holes of S2h3stcool are different among each group. From obtained Cd_i for each air holes on the combustion liner, we can calculate the effective open area of combustion liners, and estimate the pressure difference through the liner ΔP_l.

In addition, we also sampled the pressure difference through the pre-diffuser $\Delta Pdif$, and through the dump region ΔPdp as defined in Fig.3. Relation of them with the inlet air mass flow rate Wa_{cr} is shown in Fig.12, and we can see that the plots for all calculation models with the same liner configuration L2 lie on the same plot curve, even for the model with effusion cooling air holes S2h3stcool and the multi-sector model M2h3st. This means that, at least for our combustor, the pressure drop through the pre-diffuser and the dump region depends only on the total mass flow rate Wa_t, with little effect of the flow downstream.

We can now estimate ΔPdp and ΔP_l, keeping the balance between the air mass flow through fuel nozzle Wa_n and combustor liner Wa_l. Then the total pressure loss ΔPc can be obtained;

$$\Delta Pc = \Delta Pdp(Wa_t) + \Delta Pl(Wa_l) \qquad (3)$$

For the experimental models MSU2, FA1-1 and FA1-2, each effective open area of the combustor liner is estimated using Cd_i shown in Table 2, and then the total pressure loss ΔPc is estimated from equation (3) and plotted in Fig.13 denoted as "(Est.)". Plots of corresponding experimental and estimated pressure loss seem to be very close to each other.

As shown above, once the data for Cd_i in Table 2 and the relation of $\Delta Pdp(Wa_t)$ are obtained by the detailed simulation with cooling air holes, the mass flow balance of Wa_n and Wa_l, mass flow distribution and the total pressure loss can be estimated for different air hole arrangement. Furthermore, to do more accurate quantitative evaluation by the simulation, the effects of detailed configurations such as the strut of the fuel nozzle should be also evaluated.

5 SUMMARY AND FUTURE WORK

In the TechCLEAN project of JAXA, aeroengine combustors for small aircrafts have been developed. In the development process of the combustor, cost-effective cold-flow numerical simulations were utilized as support tools for the experimental research;

(1) To investigate the effect of configuration parameters on the relation between air mass flow rate and total pressure loss;
(2) To estimate the difference between multi-sector and full annular combustors;
(3) To estimate the air mass flow ratio for each group of holes, including effusion cooling air holes, on the combustion liner;
(4) Finally to estimate the effective open area and total pressure loss of the combustor.

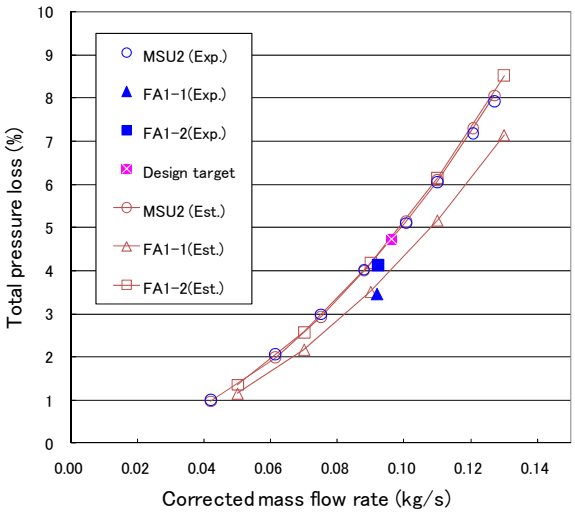

Fig.13 Comparison of experimental and estimated pressure loss. (Exp:Experimental, Est:Estimated.)

In the processes above, the cold-flow simulation suggested what was happening inside the combustor, and also the estimated values of total pressure loss were in good agreement with the experimental results. In this report, we demonstrated that, in the development process of the combustor of which flow from the air holes will largely contribute to its performance, even the cost-effective cold-flow simulation can give useful information for the combustor improvement.

For the future work, we are now trying to apply this simulation method for full annular combustor calculation to see specific characteristics of them in comparison with single-sector calculations. We would also continue to utilize numerical simulation for the combustor design, extending to take into account the spray trajectory and evaporation as much as possible.

6 REFERENCES

[1] IPCC, 1999, "Aviation and the Global Atmosphere," A Special Report of IPCC Working Group I and III.

[2] M. Makida, et al, 2006, "Preliminary Experimental Researches To Develop A Combustor For Small Class Aircraft Engine Utilizing Primary Rich Combustion Approach," ASME Paper No.GT2006-91156.

[3] M. Makida, et al, 2007, "Optimization of a Small Aircraft Combustor to Reduce NOx Emissions Under Practical Conditions," ASME Paper No. GT2007-27969.

[4] M. Makida, et al, 2008, "Verification of Low NOx Performance of Simple Primary Rich Combustion Approach

by a Newly Established Full Annular Combustor Test Facility," ASME Paper No. GT2008-51419.

[5] O'Rouke P. J., 1982, "Collective Drop Effects on Liquid Spray," Ph. D Thesis of Princeton Univ.

[6] A. K. Tolpadi, 1995, "Calculation of Two-Phase Flow in Gas Turbine Combustors," J. Eng. for Gas Turbines and Power, Vol.117, pp.695-712.

[7] R. E. Malecki, et al, 2001, "Application of an Advanced CFD-Based Analysis System to the PW6000 Combustor to Optimize Exit Temperature Distribution –Part I–," ASME 2001-GET-62.

[8] V. Sankaran, et al, 2002, "LES of Spray Combustion in Swirling Flows," J. Turbulence.

[9] CITS, 2005, "2005 Annual Technical Report," Stanford Univ.

[10] CERFACS, 2005, "Scientific Activity Report," Jan.2004-Dec.2005.

[11] N. Patel, et al, 2008, "Simulation of Spray-turbulence-flame Interactions in a Lean Direct Injection Combustor," Comb. and Flame 153, pp.228-257.

[12] S. James, et al, 2008, "Towards Improved Prediction of Aero-Engine Combustor Performance Using Large Eddy Simulations," ASME Paper No.GT2008-50199.

[13] M. Chrigui, et al, 2008, "Numerical Analysis of Spray Dispersion, Evaporation and Combustion in a Single Gas Turbine Combustor," ASME Paper No.GT2008-51253.

[14] F. Wang, et al, 2009, "Gas Turbine Combustor Simulation With Various Turbulent Combustion Models," ASME Paper No. GT2009-59198.

[15] Yu. G. Kutsenko, et al, 2009, "Modeling of Turbulent Combustion Process and Lean Blowout of Diffusion and Premixed Flames Using a Combined Approach," ASME Paper No. GT2009-60131.

[16] Lefebvre, A. H., 1998, "Gas Turbine Combustion," Second Edition, TAYLOR&FANCIS, Philadelphia.

[17] Harold C., Simmons et al, 1976, "Air-Atomizing Fuel Nozzle," United States Patent, 3980233, Sep. 14.

[18] W. I. Dodos, et al, 1990, "Combustion System Design," Chap.4 of "Design of Modern Turbine Combustors," ACADEMIC PRESS.

[19] N. Zarzalis, et al, 1992, "NOx-Reduction by Rich-Lean Combustion," AIAA PAPER 92-3339.

[20] N. K. RIZK, et al, 1993, "Three-dimensional NOx modeling for rich/lean combustor," AIAA PAPER 93-0251.

[21] Hasegawa, et al, 1997, "Effect of Pressure on Emission Characteristics in LBG-Fueled 1500C-Class Gas Turbine," ASME Paper No.97-GT-277.

[22] P. Griebel, et al, 1997, "Experimental Investigation of an Atmospheric Rectangular Rich Quench Lean Combustor Sector for Aeroengines," ASME Paper No.97-GT-146.

[23] J. W. Koopman, et al, 1998, "Investigation of a Rectangular Rich Quench Lean Combustor Sector," ASME-98-GT-230.

[24] Blomeyer, et al, 1999, "Mixing Zone Optimization of a RQL Combustor," J. of Propulsion and Power, 15, 2, March/April, pp.288-295.

[25] M. Makida, et al, 2010, "Utilization of Cold-Flow Numerical Simulation With Overset Grid Method in Development Process of Aeroengine Combustor," ASME Paper No. GT2010-23089.

[26] R. Takaki, et al, 2003, "The Development of the UPACS CFD Environment," in High Performance Computing Proceedings of 5th International Symposium, ISHPC 2003, pp307-319.

[27] Spalart, P.R., et al, 1992, "A One-Equation Turbulence Model for Aerodynamic Flows", AIAA Paper 92-0439.

[28] T. Yamane, et al, 2009, "Introduction of Combined Usage of Overset Grid Method in Conjugate Heat Transfer Simulation," ASME Paper No.GT2008-59832.